CHALMERS
UNIVERSITY OF TECHNOLOGY

Innovative flexural strengthening of RC beams using self-anchored prestressed CFRP plates: Experimental and numerical investigations

Engineering Structures 243 (2021) 112687

Contents lists available at ScienceDirect

Engineering Structures

journal homepage: www.elsevier.com/locate/engstruct

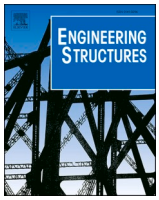

Innovative flexural strengthening of RC beams using self-anchored prestressed CFRP plates: Experimental and numerical investigations

Jincheng Yang [a], Morgan Johansson [a,b], Mohammad Al-Emrani [a], Reza Haghani [a,*]

[a] Division of Structural Engineering, Department of Architecture and Civil Engineering, Chalmers University of Technology, SE-412 96 Gothenburg, Sweden
[b] Norconsult AB, SE-417 55 Gothenburg, Sweden

ARTICLE INFO

Keywords:
Carbon fibre reinforced polymer (CFRP)
Self-anchorage
Flexural strengthening
Prestress
Reinforced concrete (RC)
Nonlinear finite element analysis
Intermediate crack-induced debonding

ABSTRACT

This paper presents an innovative method of prestressing carbon fibre reinforced polymer (CFRP) plates used as externally bonded reinforcement for flexural strengthening of reinforced concrete (RC) beams. The proposed method aims to achieve self-anchorage of the prestressed CFRP plate and thus eliminate the need for conventional mechanical anchorage at its ends. Experimental tests of RC beams in four-point bending were conducted to investigate the strengthening efficiency of the self-anchored prestressed CFRP plate. The experimental results showed that using the self-anchored prestressed CFRP significantly improved the flexural performance of the strengthened beam in terms of bending stiffness, crack widths, and load-carrying capacity. The utilisation ratio of the prestressed CFRP plate reached 81% at its debonding. Numerical analyses using nonlinear finite element (FE) method were conducted to model the tested specimens. Based on the reliable simulation of flexural cracks and crack-induced CFRP debonding, parametric studies were conducted using FE analyses, in order to investigate the effect of prestressing levels and the CFRP plate's stiffness on the flexural behaviour. Recommendations were then made for selecting a proper prestressing level and the mechanical properties of CFRP plates.

1. Introduction

Using carbon fibre reinforced polymer (CFRP) plates as externally bonded reinforcement (EBR) has become a commonly accepted technique for enhancing the flexural capacity of deficient structures made of different materials, including concrete [1–4], steel [5–8] and timber [9]. A major problem associated with conventional EBR is the premature separation of the bonded plates from the strengthened structural elements, known as "debonding". Debonding is often triggered at stress concentration locations such as plate ends where shear lag effect exists [4,7]. In reinforced concrete (RC) structures, the stress concentration also occurs at the locations of cracks (due to bending or shear) causing "intermediate crack (IC)" debonding. Debonding of EBR is generally an unfavourable failure mode since it greatly reduces the strengthening efficiency and utilisation of the plate. For instance, only about 20–30% of the tensile capacity of CFRP plates is utilised when used as EBR for flexural strengthening of RC structural elements [11]. Furthermore, conventional EBR using passive (non-prestressed) CFRP plates does not notably improve the performance of strengthened RC beams in serviceability limit state (SLS) regarding the bending stiffness and crack widths.

To increase the effectiveness of using bonded CFRP plates, researchers have proposed prestressing them before bonding to the structure [10,11]. Compared to unstressed CFRP plates, introducing prestress to the plates could significantly improve the flexural performance in SLS, further enhancing the flexural capacity in ULS and obtain greater utilisation of the CFRP plate at debonding [14,15].

To prevent premature debonding of prestressed plates, it is essential to have proper anchorage at the ends of the plates [12,13]. In the absence of end anchorage, the prestressed plate would peel off from the concrete surface once the prestressing device is removed, due to large interfacial stresses close to the ends of the bonded plate [16]. To anchor the bonded FRP reinforcement used for flexural strengthening, researchers have investigated various type of anchorage systems, such as mechanically fastened metallic anchors [17–19], FRP U-jackets [20–22], and FRP (spike) anchors [23–26]. Further information about different anchorage systems is available in reviews by Kalfat et al. [27] and Grelle & Sneed [28]. Mechanical anchorage systems composed of metallic plates and bolts are the earliest form of anchorage devices studied by researchers [27]. It is commonly used to anchor the prestressed plates to concrete surface and assure a safe force transfer. Although metallic anchor plates could provide satisfying anchorage

* Corresponding author.
E-mail address: reza.haghani@chalmers.se (R. Haghani).

https://doi.org/10.1016/j.engstruct.2021.112687
Received 2 February 2021; Received in revised form 16 April 2021; Accepted 3 June 2021
Available online 17 June 2021

capacity, their application might be associated with several drawbacks: (a) labour-intensive installation process involved with cutting and drilling concrete to install the metallic plates and bolts; (b) steel anchors' vulnerability to corrosion during the service life; (c) restrictions in the inspection of anchors due to lack of access (i.e. anchors cannot be opened); (d) sensitivity to the quality of workmanship; and e) aesthetic aspects and vandalism issues.

To avoid these problems, Stöcklin and Meier [29] suggested a gradient anchorage method to self-anchor prestressed plates. The gradient anchorage is realised by the segmental release of the prestressing force over a certain length at each end of the plate, referred to as "anchorage length". The prestressing force in each segment is released with the aid of (a) a computer system controlling the hydraulic jack and (b) a fast curing device using elevated temperature to prepare for application of the next segment [30]. This process continues until the prestressing force is reduced to zero at the end of the plate. Thus, the prestressing force exhibits a gradually decreasing profile towards the plate ends along the anchorage length. The gradually decreasing prestressing force is meant to reduce interfacial stresses occurring in the bond line. These reduced interfacial stresses may be carried by the adhesive bond strength between the CFRP and concrete. This method was applied to a pilot project in Poland in 2014 [31]. Despite the successful concept, the computer-controlled prestressing and fast curing systems add complexities to the method. The multi-step procedure for prestressing and curing requires rather a long time and involves the use of certain epoxy adhesives with a long pot life.

To realise self-anchorage, Haghani et al. [32] proposed an innovative, "stepwise prestressing" method and a mechanical tool with a simple operational procedure. Unlike the gradient anchorage method which releases the prestressing force in multiple steps, the stepwise prestressing method creates the desirable force profile by adding up the prestressing force in multiple steps in one act by using a purely mechanical tool. Previous experimental investigations [33] demonstrated successful self-anchorage of externally bonded CFRP plates with prestressing levels of up to 33% (of the CFRP tensile capacity).

Using experimental and numerical approaches, this paper investigates the flexural behaviour of RC beams strengthened with bonded CFRP plates using the stepwise prestressing method. Experimental results are presented and discussed in terms of load–deflection behaviour, bending stiffness, crack widths, failure modes, and utilisation of the CFRP plate. Numerical analyses based on the finite element (FE) method were conducted as an efficient approach to the verification and optimisation study of the FRP-strengthened RC beams. Suitable modeling strategies for carrying out FE simulations on FRP-strengthened concrete structures were recently reviewed by Naser et al. [34]. In the current study, two-dimensional (2D) models of the tested specimens were developed in the commercial FE package ABAQUS [35] to provide reliable simulation of flexural cracks and the IC debonding of the CFRP plate. Based on the FE analyses, parametric studies were conducted to further investigate the effect of prestressing levels and the elastic modulus of the CFRP plate on the flexural behaviour of the strengthened RC beams.

2. Experimental programme

In the current study, the experimental programme consisted of three RC beams tested to failure in four-point bending. The flexural tests aimed to (a) investigate the strengthening efficiency of the self-anchored prestressed CFRP plate in the flexural behaviour of the strengthened beam and (b) evaluate the utilisation ratio of the self-anchored CFRP plate at failure.

2.1. Specimens and test set-up

The dimensions of the three RC beams and test set-up is shown in Fig. 1. Two steel reinforcement bars (B500C, ribbed, Φ16) were used on both the tensile and compressive side of the beams. Stirrups (B500C, ribbed, Φ10) were evenly spaced over the entire length of the beams, with a spacing of 75 mm. Upon the arrival of these three RC beams at the laboratory, cracks were observed caused by shrinkage and unexpected loading during transportation; the maximum crack width in each beam was approximately 0.2 mm. The first beam (B1) was not strengthened and served as a reference specimen. The second beam (B2) was externally bonded with a passive (non-prestressed) CFRP plate. The third beam (B3) was pre-loaded in four-point bending under a load of 30 kN, equivalent to 50% of the theoretical yielding load. After removing the pre-loading, B3 was strengthened with a prestressed CFRP plate using the stepwise prestressing method. The pre-loading of B3 aimed to induce pre-cracks before the strengthening and thus provide the opportunity to investigate the efficiency of using the prestressed CFRP plate in improving bending stiffness of cracked sections and reducing crack widths in the SLS. The CFRP plates used in B2 and B3 were 3.8 m long with a cross-section of 80 × 1.45 mm^2.

After preparation, the specimens were simply supported on two steel roller supports, providing an effective span of 4.2 m. Two equal point loads were applied on the specimens creating a constant-moment span of 1.3 m. The loads were applied in a displacement-controlled manner at a rate of 1 mm/min measured at the midspan. To obtain the net deflection at midspan, three linear variable differential transducers (LVDTs) were used; LVDT 2 at the midspan and LVDT 1 and 3 at the centre of each support. In the two CFRP-strengthened beams, strain gauges were installed on the CFRP plates to monitor the development of the axial strain. In specimen B2, two strain gauges were installed at the middle of the bonded CFRP plate. However, 19 strain gauges were installed in specimen B3 to monitor axial strains in the prestressing phase and flexural test, see Fig. 1. Crack widths at the height of tensile reinforcement were measured with a handheld digital microscope at load levels of 15, 30, 45, 55 (B1 only), and, further, at 70 kN (B2 and B3 only).

2.2. Self-anchored prestressed CFRP plate on B3

A detailed operational procedure for applying the self-anchored prestressed CFRP plate was introduced in a previous publication [32]. In the prestressing phase, the maximum tensile force reached 100 kN. At that moment, the maximum tensile strain measured in the midspan

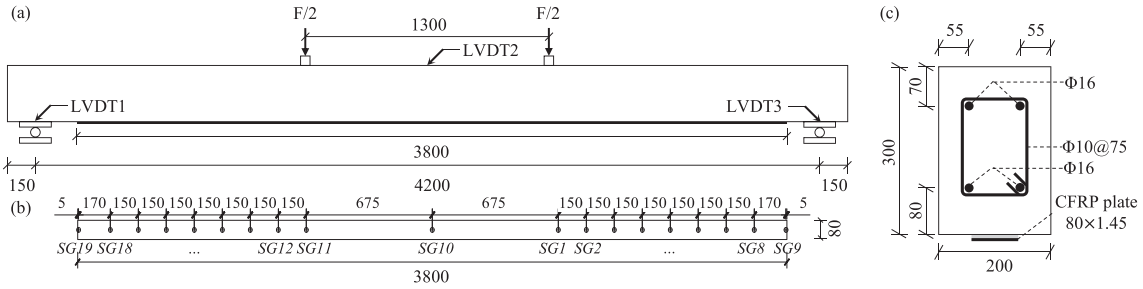

Fig. 1. (a) Test set-up for specimens subjected to four-point bending; (b) bottom view of the self-anchored prestressed CFRP plate on specimen B3 with 19 strain gauges installed along its length; (c) cross-sectional dimensions of the RC beams with bonded CFRP plate (All dimensions are in mm).

section of the CFRP plate was 4.0‰, corresponding to a prestressing level of 31% (of the ultimate strain ε_{fu} of the plate). The midspan tensile strain dropped to 3.6‰ after 24 h of curing the epoxy adhesive between the CFRP plate and concrete and then decreased to 3.5‰ (27% of ε_{fu}) after removing the prestressing system six days afterwards. Before being subjected to the flexural test, the maximum prestressing level of the CFRP plate was 27%. At such a prestressing level, the self-anchorage of the prestressed plate was achieved without the need for mechanical end anchorage, as shown in Fig. 2.

2.3. Material properties

The three RC beams were supplied by a local workshop using concrete C35/45. The concrete grade was verified by compressive tests of concrete cylinders cut from the beams using a core drill after the flexural testing. The concrete compressive strength f_c, tensile strength f_{ct}, and elastic modulus E_c on the testing day were determined as 51.1 MPa, 3.6 MPa, and 36.9 GPa, respectively, based on the properties of concrete C35/45 provided in EN 1992-1-1:2004 [36]. The fracture energy G_F was estimated to be 148 N/m according to Model Code 2010 [37]. The steel reinforcement used in the beams was B500C hot-rolled ribbed bars. Based on the standard tensile test according to ASTM A615/A615 M [38], the elastic modulus E_s, yield strength f_{sy}, ultimate strength f_{su} and ultimate strain ε_{su} of the main reinforcement bars were measured at 201 GPa, 510 MPa, 618 MPa and 12.0%, respectively. The CFRP plates used in the current study were pultruded sections with unidirectional carbon fibres (StoFRP IM 80C supplied by sto®). The material properties of the CFRP plates were obtained based on the standard tensile tests following ASTM D3039 [39]; the elastic modulus E_f and ultimate tensile strain ε_{fu} were measured at 214 GPa and 12.7‰, respectively. A two-component epoxy adhesive (StoPox SK41 supplied by Sto®) was used to bond the CFRP plate to the concrete surface. Based on the tests conducted on dog-bone samples cured at room temperature [40], the elastic modulus E_a and tensile strength f_a of the epoxy were determined as 7.1 GPa and 34 MPa, respectively. The Poisson's ratio v_a was assumed to be 0.3. The design thickness of the adhesive layer t_a was 1 mm.

3. Numerical analysis

Numerical analyses were carried out as nonlinear FE modelling using a commercial package, ABAQUS/CAE [35]. The goal of the numerical analyses was to provide reliable predictions of the IC debonding of CFRP plates and recommendations for optimising the application of pre-stressed CFRP plates based on parametric studies. To achieve the goal, it was critical in the current FE analyses to (a) properly model the nonlinear behaviour of concrete in tension, (b) reasonably define concrete compressive behaviour to avoid underestimating its resistance to crushing, and (c) consider relative slip in the bond of concrete-to-steel reinforcement and concrete-to-CFRP plate.

In the current study, two-dimensional (2D) models were developed for the three specimens subjected to four-point bending. Considering that the specimens and test configurations were symmetric about the midspan section, only half of each specimen was modelled to save computational time. Concrete and CFRP plates were modelled as 2D shells, discretised into structured meshes, and assigned element type CPS4 (four-node plane stress quadrilateral elements with four integration points). Concrete material was defined using a concrete damage plasticity (CDP) model. Steel reinforcement and CFRP plates were modelled as one-dimensional (1D) wire; *Truss* (T2D2) and *Beam* (B21) elements were assigned to steel reinforcement and CFRP plate, respectively. The adopted modelling strategy and options were comprehensively described and validated in a previous study [41]. Critical issues are briefly introduced below.

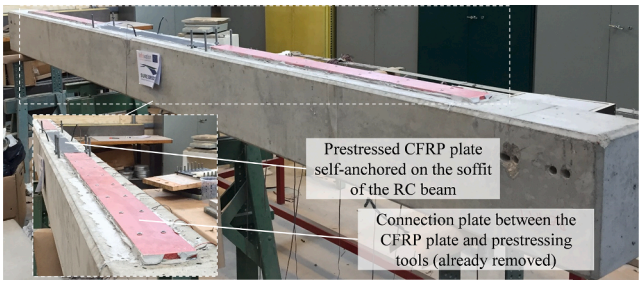

Fig. 2. Self-anchored prestressed CFRP plate on the RC beam (specimen B3) after removing the stepwise prestressing tools [32].

3.1. Modelling of concrete

The tensile behaviour of concrete was defined using a linear elastic curve before reaching concrete tensile strength f_{ct} and a bilinear softening curve in the post-peak regime, according to the stress-crack width relationship provided in Model Code 2010 [37], see Fig. 3. The smeared crack method was adopted in the concrete model to simulate the nonlinear deformation of cracking concrete. The cracking concrete was treated as a continuum and the crack opening w_{cr} was described as an equivalent cracking strain ε_{cr} smearing over a certain length (referred to as smeared length l_s). To ensure the objectivity of the smeared crack method, the assumed smeared length l_s should represent the actual size of simulated cracking zones in the concrete continuum which, in the current FE analyses, was equal to the crack band width h_b of damaged concrete elements running across the concrete mesh. Considering that the simulated crack bands were perpendicular to the span direction (due to dominant bending effects in the tested specimens) the crack band width h_b was determined as the width of square-shaped concrete elements [42,43].

The concrete compressive behaviour was defined based on a stress–strain relationship in Model Code 90 [44]. Using the original Model Code stress–strain relationship (smearing compressive deformation over the whole length L of 200-mm-long concrete specimens [44]) might underestimate resistance to concrete crushing failure in the critical fracture damage zone with an actual length L_{cr} less than 200 mm, see Fig. 4(b). Hence, the original post-peaking descending branch was modified to better describe the dissipated energy of compressive concrete per unit volume within L_{cr}. The modification principle is illustrated in Fig. 4(a) [41]. According to the parametric study of L_{cr} in the range from 40 to 200 mm, the actual size of the simulated crushing zone matched the assumption for L_{cr} as an input, only if L_{cr} was set to 100 mm [41]. Accordingly, the length of the critical crushing zone in the FE analyses was determined as 100 mm.

3.2. Steel reinforcement, CFRP plate, and bond behaviour

The stress–strain diagrams of steel reinforcement bars and CFRP plates, adopted for material modelling, are shown in Fig. 5. *Connectors* (translator) were used to build the node-to-node connections between

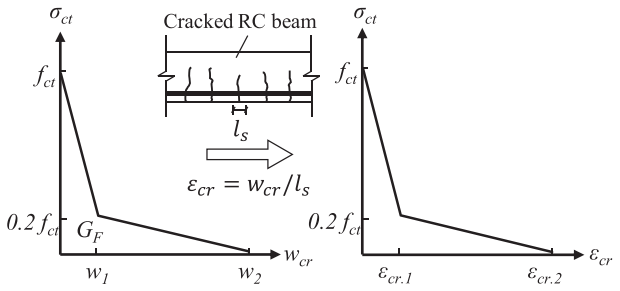

Fig. 3. Bilinear softening curve defined for the post-peak tensile behaviour of concrete converted from stressσ_t-crack width w_{cr} relationship according to Model Code 2010 [37].

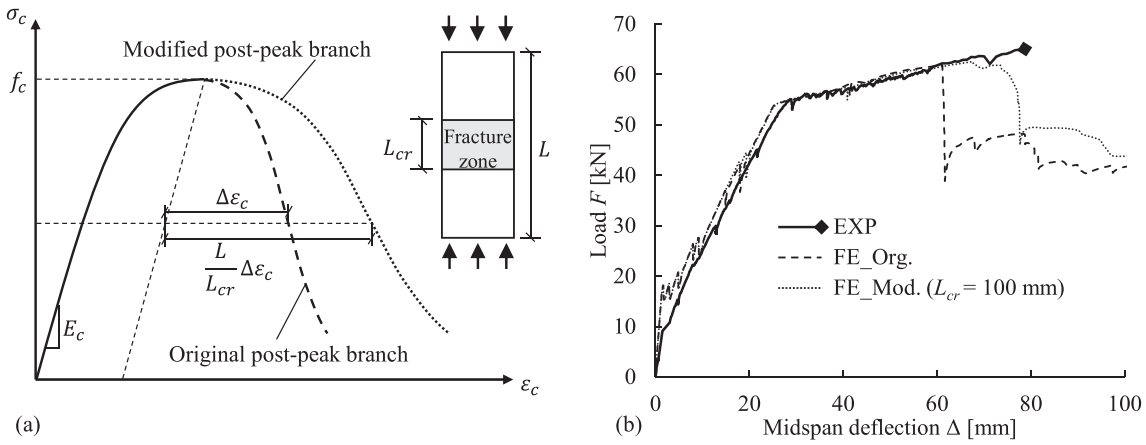

Fig. 4. (a) Modification of post-peak branch to consider strain-softening behaviour in local fracture zone of concrete specimens in compressive tests [41]; (b) load–deflection curves of the reference specimen B1 including experimental measurements (EXP), FE analysis using the original post-peak branch of Model Code relationship (FE-Org.) and FE analysis using modified post-peak branch, given L_{cr} = 100 mm (FE-Mod.)

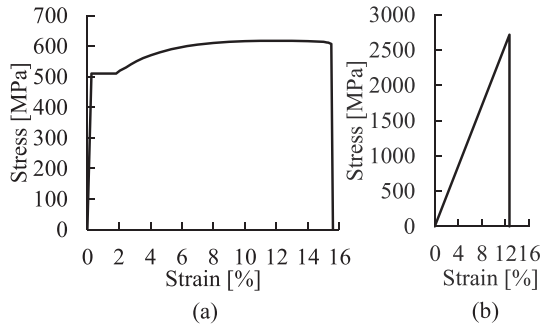

Fig. 5. Stress–strain relationship assigned to (a) steel reinforcement and (b) CFRP plates in FE analyses.

the main reinforcement bars and surrounding concrete, according to the method proposed in [41]. These *connectors* were assigned a force-slip relation, to represent the bond stress-slip curve according to Model Code 2010 [37], see Fig. 6(a). The bond layer between concrete and CFRP plates was modelled with cohesive elements. The constitutive behaviour of cohesive elements was defined using the traction-separation law including damage evolution to represent the bond-slip model proposed by Lu et al. [45], see Fig. 6(b). A cohesive element would be removed during the analysis once it was fully damaged.

3.3. Modelling of the prestressed CFRP plate

In the FE model of specimen B3, axial strains in the prestressed CFRP plate were modelled by inducing thermal contraction of the CFRP in a stepwise manner over multiple segments. To represent the pre-strains induced by the eight discrete point loads from the prestressing tool [16], the CFRP plate was first fixed (the degrees of freedom were constrained) at the positions of these point loads. Instead of assigning point loads, a coefficient of linear thermal expansion was defined in the material properties of the CFRP plate. In each segment of the CFRP, a proper negative temperature was defined to induce the thermal contraction and thus obtain the pre-strain comparable to the value measured by the corresponding strain gauges in specimen B3. After activating the adhesive layer between CFRP and concrete beam in the FE model, the constrains of the CFRP plate were removed in the subsequent steps to allow the force re-distribution between the prestressed CFRP plate and concrete beam, which resembled the removal of prestressing tool in specimen B3 and the consequent self-anchorage of the prestressed CFRP plate. After the force re-distribution step, the axial strain along the length of the self-anchored CFRP plate in the FE model is shown in Fig. 7, in comparison with axial strains measured by the 19 strain gauges in specimen B3. The comparison in Fig. 7 showed that the prestressing level induced by the thermal contraction method in the FE model closely matched the prestressed state of the CFRP plate in specimen B3.

3.4. Numerical solution strategy

In the nonlinear FE analysis of concrete solved in a static procedure,

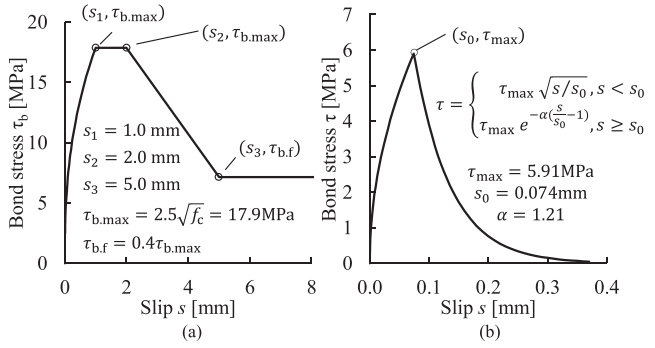

Fig. 6. Adopted bond-slip relationship (a) between concrete and internal steel reinforcement according to Model Code 2010 [37] and (b) between concrete and the CFRP plate, according to the model proposed by Lu et al. [45].

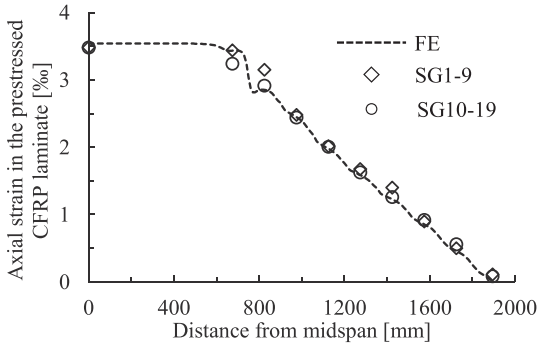

Fig. 7. Axial strains in the prestressed CFRP plate of specimen B3: comparison between the FE modelling (FE) and the experimental measurement by strain gauges (SG1-19).

convergence difficulties are commonly observed due to the strain-softening and stiffness degradation of damaged concrete [35]. In the current FE analyses, the technique of viscoplastic regularisation was implemented to effectively solve the convergence difficulties in the static solution procedure. Viscoplastic regularisation was introduced by specifying viscosity parameter μ as a plasticity factor of concrete. The defined value of μ should be relatively smaller than the characteristic increment size in numerical analysis [35] to improve the convergence rate without compromising on simulation accuracy in, say, flexural behaviour and cracking in concrete. Based on a parametric study of μ in the range $1 \times 10^{-3} - 1 \times 10^{-10}$ [41], μ was set to 1×10^{-6} in the current FE analyses, to obtain satisfying convergence rates with reliable results.

3.5. Mesh sensitivity analysis

Besides the convergency difficulties, a mesh sensitivity analysis was conducted to assure the independence of numerical results on concrete element sizes. As shown in Fig. 8, the concrete continuum of each model was discretised into square elements with sizes (side lengths) from 10 to 40 mm. Given a size of no more than 30 mm, individual crack bands developed and localised in single rows of concrete elements; simulated load–deflection curves were not sensitive to the mesh discretisation. Concerning accuracy and computational efficiency, the square element size of 20 × 20 mm^2 was selected in the current FE modelling.

4. Experimental and numerical results

The strengthening efficiency of the self-anchored prestressed CFRP plate was evaluated based on experimental results concerning flexural behaviour, crack widths, and utilisation of the plate. For verification, the simulated cracking behaviour and IC debonding of the CFRP plate were compared with the experimental measurement.

4.1. Flexural behaviour

Current flexural tests showed that using bonded CFRP plates (especially the self-anchored prestressed CFRP plates using stepwise prestressing) effectively improved the flexural stiffness and load-carrying capacity of specimens B2 and B3 in comparison with the reference specimen B1, whereas the ultimate deflection at failure was reduced after the CFRP-strengthening. Fig. 9 provides an overview of the flexural behaviour of the specimens, including load–deflection curves from both experimental measurements and FE analyses. Considering that pre-cracks before flexural tests were not modelled in the current FE analyses, the FE results exhibited stiffer flexural responses in the initial phase with clear cracking stages.

In the reference specimen B1, flexural failure was initiated by concrete crushing on the compressive side of the beam in the constant-moment span. At the moment of observing concrete crushing, external loads on specimen B1 were removed for laboratory safety reasons. Unlike B1, the failure mode of the two CFRP-strengthened specimens B2 and B3 was CFRP debonding induced by intermediate cracks (IC debonding). Fig. 10 shows the IC debonding took place in B2 (with a passive CFRP plate) and B3 (with a self-anchored prestressed CFRP plate). It is worth noting that the rupture of the CFRP plate in B3 was caused by great energy released at the moment of debonding failure. At the debonding failure moment, the ultimate load capacities of B2 and B3 were enhanced to 63% and 126% higher, respectively, than that of the reference specimen B1. However, the ultimate deflection of B2 and B3 was reduced significantly. The ultimate load and deflection of the three specimens and their failure modes are summarised in Table 1.

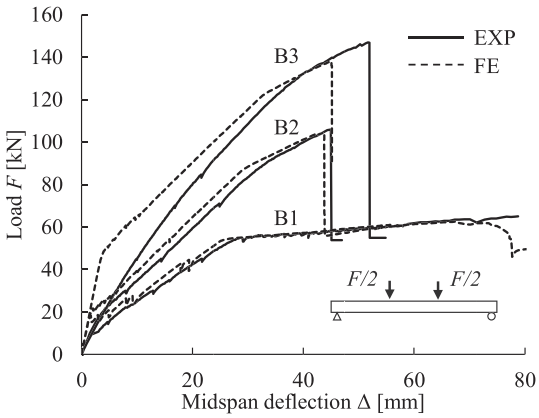

Fig. 9. Flexural behaviour of all specimens in four-point bending tests; load–deflection curves according to experimental measures (EXP) and FE analyses (FE).

4.2. Development of crack widths

Compared with reference specimen B1, using the bonded CFRP plates in specimens B2 and B3 led to (a) slightly reduced growth rates of crack widths, (b) postponed fast increase of crack widths at the yielding of steel reinforcement, (c) reduced mean value of crack widths due to an increased number of cracks, and (d) closed pre-cracks in specimen B3 due to the prestressing force in the CFRP plate.

Fig. 11 shows the maximum and mean value of crack widths within the constant-moment span of the specimens measured at loads of 0, 15, 30, 45, 55 kN (B1 only), and, further, at 70 kN (B2 and B3). For the maximum crack width of each specimen, the width of the same crack is plotted in Fig. 11(a). It should be noted that the crack width plotted for B1 was not the largest opening until 55 kN. This explained why the maximum crack width of B1 plotted in Fig. 11(a) was even smaller

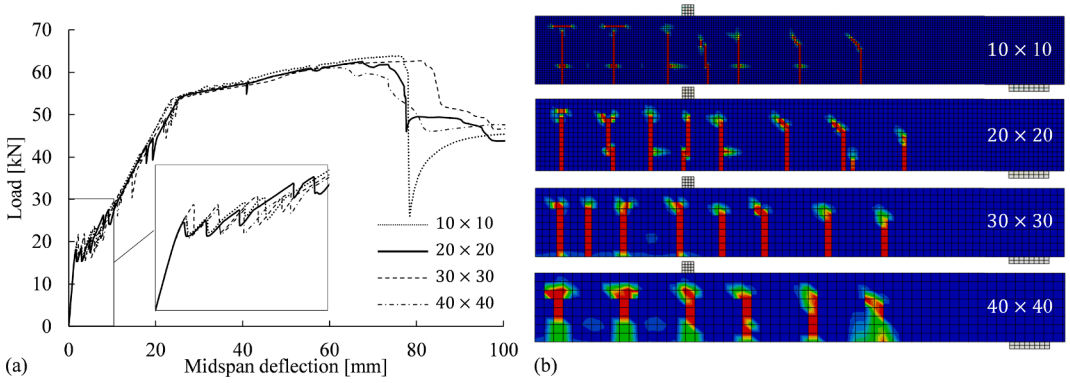

Fig. 8. (a) Load-deflection curves and (b) crack patterns in the FE analyses of the reference specimen B1, using square-shape concrete elements with side lengths of 10, 20, 30, and 40 mm.

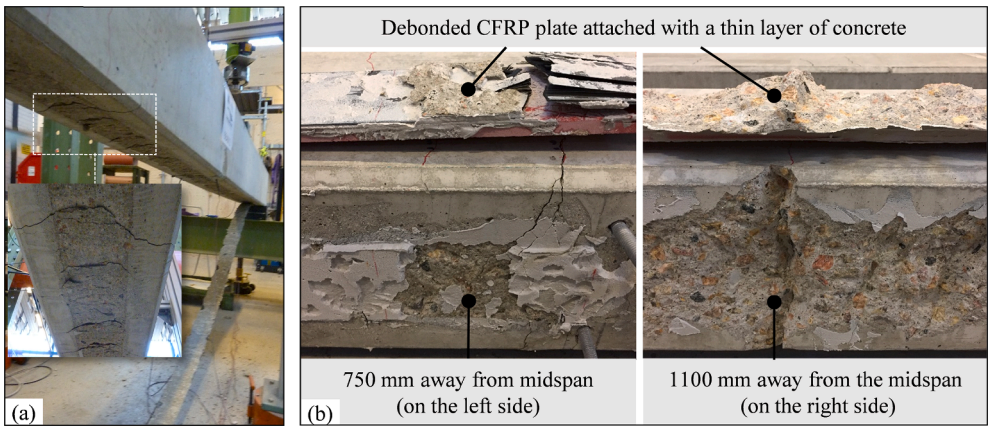

Fig. 10. IC debonding of the CFRP plate in (a) specimen B2 and (b) specimen B3.

Table 1
Ultimate load and midspan deflection at the failure of tested specimens according to experimental measurements (EXP) and FE analyses (FE).

Specimen	Results	F_u [kN]	Δ_u [mm]	Failure mode
B1	EXP	65.0	78.7	CC
	FE	61.1	73.8	CC
B2	EXP	105.8	45.0	IC
	FE	104.5	43.8	IC
B3	EXP	146.9	51.7	IC
	FE	137.9	45.0	IC

Notes: F_u and Δ_u = load and deflection capacity at ultimate state; CC = concrete crushing; IC = CFRP debonding induced by intermediate cracks.

before 45 kN than the mean value of B1 in Fig. 11(b). Before loading, the maximum crack widths in the reference specimen B1 and passive-CFRP-strengthened specimen B2 were approximately 0.2 mm, due to shrinkage and, possibly, unexpected loading during transport. However, pre-cracks induced in specimen B3 were closed due to the compressive force from the prestressed CFRP plate. In the loading phase, the growth rate of the maximum crack width in B2 and B3 was smaller than that of reference specimen B1 due to the bonded CFRP plate. The mean crack width in B2 even reduced at 45 kN, due to the increase in crack numbers at the constant-moment span from 6 (at 30 kN) to 10 (at 45 kN). The increase in crack numbers in the CFRP-strengthened specimens is demonstrated in Fig. 13. The rapid increase in crack width in B1 at the load of 55 kN did not take place in CFRP-strengthened specimens B2 and B3 due to the postponed yielding of steel reinforcement. In specimen B3, the applied prestressed plate effectively closed the pre-cracks, thus preventing the maximum crack width from becoming the governing design parameter in SLS.

4.3. Utilisation of CFRP plates

Axial strain in the CFRP plate was monitored by strain gauges. Fig. 12 shows the development in axial strain at the midspan of the strengthened specimens, B2 and B3. The strain gauge in B2 was damaged at a load of 98.2 kN. A linear extrapolation (black dotted line in Fig. 12) was conducted to extend the curve, until the failure load of 105.8 kN. Thus, the maximum tensile strain in the CFRP plate was estimated as 5.9‰ in specimen B2, equivalent to a utilisation ratio of 47%. In specimen B3, although the prestressed CFRP plate was self-anchored without mechanical end anchors, the tensile strain at the midspan of the plate reached 10.3‰ at debonding failure, corresponding to a utilisation ratio as high as 81%. The improved 34% utilisation ratio

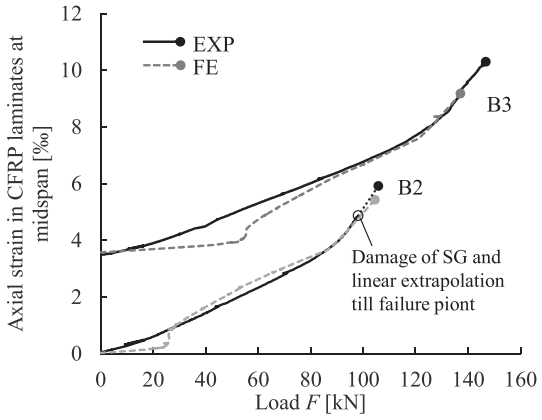

Fig. 12. Development of the axial strain in the CFRP plate at midspan section, during loading of specimens B2 and B3.

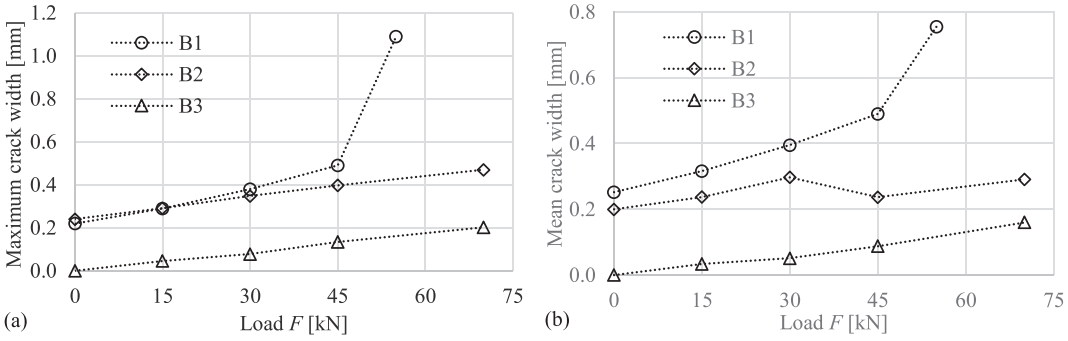

Fig. 11. (a) Maximum and (b) mean value of crack width in the constant-moment span of the specimens measured at loads of 0, 15, 30, 45, 55 kN (B1 only), and 70 kN (B2 and B3 only).

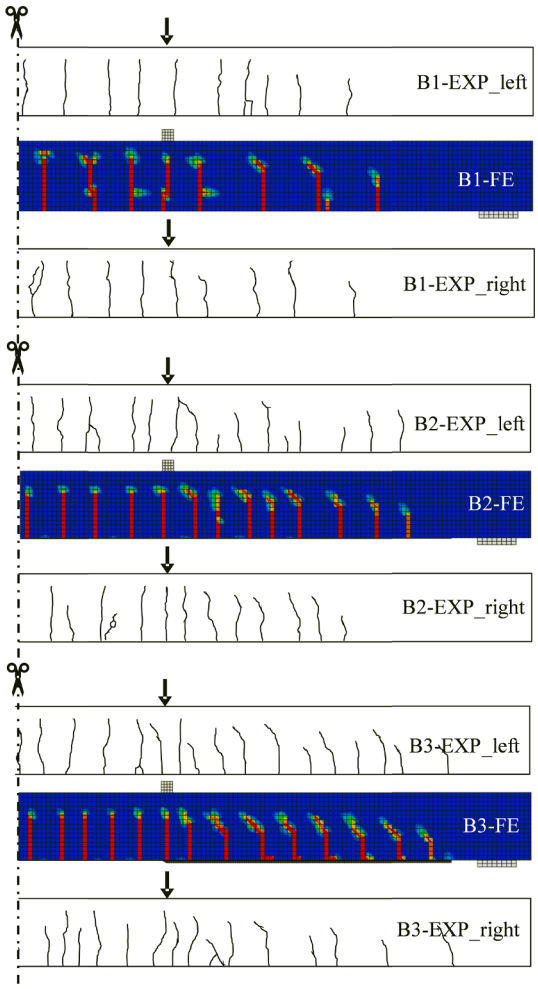

Fig. 13. Crack patterns in experimental specimens B1-B3 and corresponding FE models at the moment of failure.

was mainly attributed to the initial prestressing level of 27%.

4.4. IC debonding in FE analyses

Initiation of the IC debonding is closely related to the development of flexural cracks in the specimens. To assure a reliable prediction of IC debonding in the FE analyses, it was critical to accurately simulate the cracking behaviour of the tested beams, especially crack widths after the yielding of steel reinforcement. Fig. 13 shows crack patterns formed in the three specimens and their simulation in the FE models at the moment of failure. In general, the simulated crack patterns were comparable to the experimental observations. The increased number of flexural cracks in the tested specimens was well captured by the FE analyses showing, for example, eight cracks in the constant-moment region of B1, 10 in B2, and 12 in B3. The crack widths were also compared between the experimental measurements and FE modelling. Fig. 14 shows the crack width in the constant-moment span of B1 and B2, measured at the highest load levels of 55 kN and 70 kN respectively. Although the experimental measurements exhibited larger scattering, the mean crack width values lay well between experimental and numerical results. The reliable simulation of crack widths served as the foundation of reliable predictions of the IC debonding in B2 and B3, which took place at deflections comparable to those of the tested specimens, as shown in Fig. 9. As an example, the IC debonding of the CFRP plate in the FE analyses of specimen B2 is shown in Fig. 15.

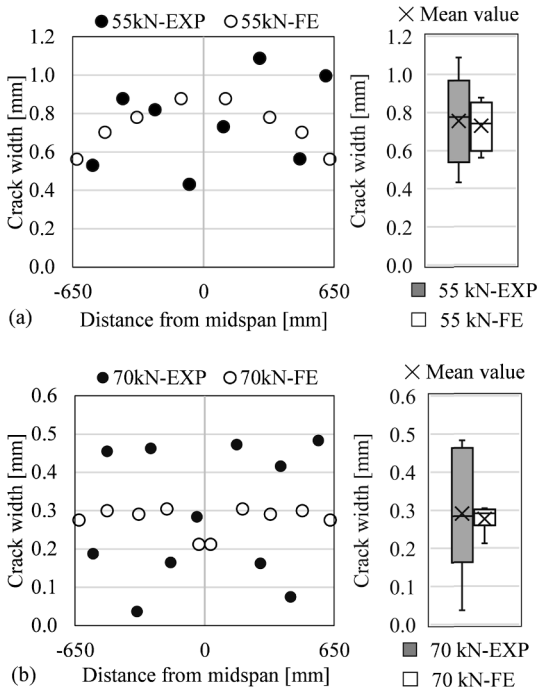

Fig. 14. Crack widths in the constant-moment span of (a) B1 at the load of 55 kN and (b) B2 at the load of 70 kN, including comparison in box-and-whisker plots.

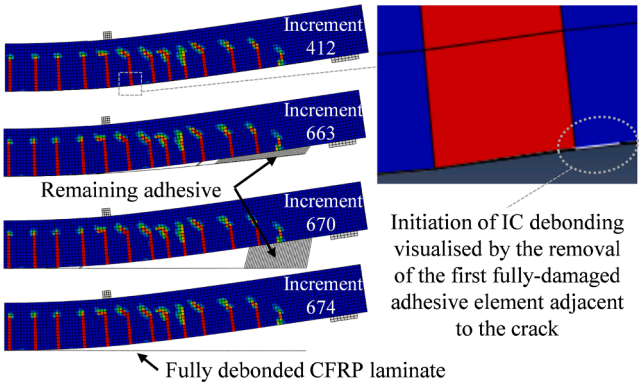

Fig. 15. Example showing initiation and development of IC debonding in the FE analysis of specimen B2.

5. Parametric study on strengthening with prestressed CFRP plates

Based on the verified FE models, parametric studies were conducted to investigate the effects of the prestressing level and elastic modulus of the CFRP plate on the flexural behaviour of a strengthened beam. The parametric studies aimed to provide an insight into the optimised application of a prestressing CFRP plate for flexural strengthening. It is worth noting that *ductility* in the following discussion refers to the deflection ductility index μ_Δ, calculated as:

$$\mu_\Delta = \Delta_u / \Delta_y \tag{1}$$

where Δ_y is the deflection at the yielding of steel reinforcement and Δ_u is the ultimate deflection at the CFRP debonding failure.

5.1. Prestressing level

In the design of bonded prestressed CFRP systems, one of the most

important parameters to determine is the prestressing level. A parametric study was carried out, covering the prestressing level in a range from 0 to 50% (of the CFRP tensile strength). The results, in terms of load–deflection curves, are presented in Fig. 16. A higher prestressing level effectively increased the cracking load in SLS. Given a prestressing level of up to 40%, the flexural failure was governed by the IC debonding after yielding of steel reinforcement. The increase in prestressing level enhanced the ultimate load capacity. Considering the limited change of ultimate deflection and the postponed yielding point, the ductility decreased at a higher prestressing level. However, when the prestressing level reached 50%, the IC debonding took place even before yielding of the steel reinforcement. As a result, both ultimate load and ductility were reduced, compared with the case that had a 40% prestressing level. The parametric study indicated that, for the RC beams in the current study, choosing a prestressing level within 40% was a compromise between ultimate load capacity and ductility. However, increasing the prestressing level to 50% or higher would add no benefits in ultimate limit state.

5.2. Elastic modulus of CFRP plates

Commercially available CFRP plates, in the form of pultruded plates, usually have elastic moduli in the range of 170–230 GPa. The larger the elastic modulus, the higher the cost of the CFRP product. Four values of the elastic modulus were evaluated in the parametric study, as shown in Fig. 17. The comparison of load–deflection curves showed that using a stiffer CFRP plate provided limited improvement in the cracking load, flexural stiffness, and load capacity. However, the increase in elastic modulus reduced the ductility, owing to the delayed yielding point and reduced ultimate deflection at debonding failure. Therefore, using a CFRP plate with low elastic modulus might be a good strategy for increasing the ductility of the strengthened beam while reducing the material cost of CFRP plates.

6. Conclusion

This paper investigated a novel technique to prestress CFRP plates used as EBR for flexural strengthening of RC beams. Using the proposed "stepwise prestressing" technique allowed safe self-anchoring of prestressed CFRP plates (given a prestressing level of 27% of the CFRP tensile strength), without the need for mechanical anchorage. An experimental programme using four-point bending tests was carried out to further study the effectiveness of the prestressing technique in terms of the flexural behaviour of the strengthened beams. Numerical analyses based on nonlinear FE modelling were conducted to provide recommendations for selecting the prestressing level and mechanical properties of CFRP plates.

6.1. The following conclusions may be drawn from this study:

The flexural tests showed that even though the beam in specimen B3 was pre-cracked before strengthening, using the prestressed CFRP plate enhanced the bending stiffness by 103% and 43% compared with the reference specimen B1 and specimen B2 (strengthened with a passive CFRP), respectively.

Using the prestressed CFRP plate in specimen B3 effectively reduced crack widths, due to the compressive force and consequent cambering effect in the concrete beam in the prestressing phase and delayed the yielding of steel reinforcement.

A higher utilisation ratio was achieved in the self-anchored prestressed plate than that of the passive CFRP plate. Flexural tests showed that the utilisation ratio of the CFRP plate increased from 47% in specimen B2 to 81% in specimen B3.

Using the prestressed plate further increased the load-carrying capacity, compared with strengthening with passive CFRP plate. The ultimate load capacity of specimen B3 was 39% higher than that of specimen B2.

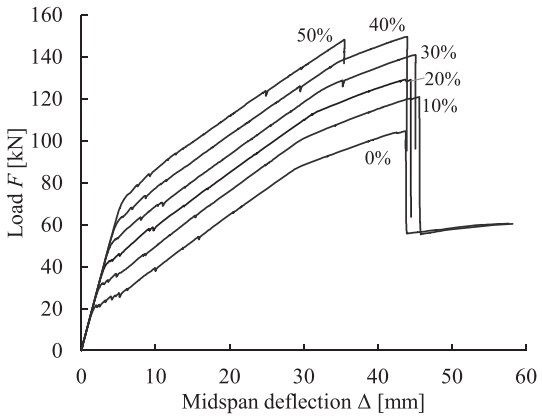

Fig. 16. Parametric study of prestressing levels from 0 to 50% (of CFRP tensile capacity): load–deflection curves of CFRP-strengthened RC beams based on the FE modelling of specimen B3.

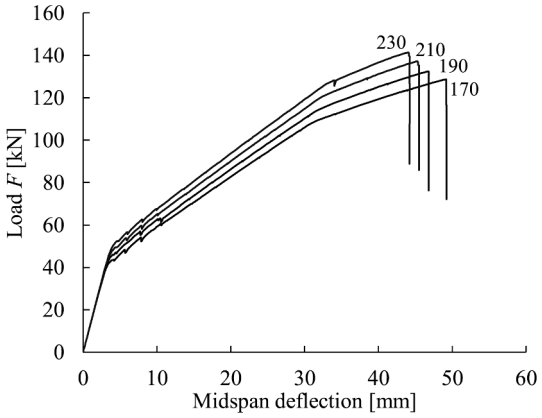

Fig. 17. Parametric study of elastic modulus of CFRP plates from 170 to 230 GPa: load–deflection curves of CFRP-strengthened RC beams based on the FE modelling of specimen B3.

Parametric studies showed that using too high a prestressing level might offer no benefits in either ultimate load or deflection capacity, owing to that the IC debonding would take place earlier than yielding of steel reinforcement. Reducing the prestressing level or elastic modulus of CFRP plate would be an effective approach to increase deflection capacity, given that the reduction in ultimate load capacity was acceptable.

Uncited reference
[13].

CRediT authorship contribution statement

Jincheng Yang: Conceptualization, Methodology, Validation, Formal analysis, Investigation, Data curation, Visualization. **Morgan Johansson:** Supervision. **Mohammad Al-Emrani:** Supervision. **Reza Haghani:** Conceptualization, Methodology, Validation, Investigation, Data curation, Resources, Supervision, Project administration, Funding acquisition.

Declaration of Competing Interest

The authors declare that they have no known competing financial interests or personal relationships that could have appeared to influence the work reported in this paper.

Acknowledgements

The work in the paper is a part of SUREBridge (Sustainable Refurbishment of Existing Bridges) project which has received funding from the European Union's Seventh Framework Programme for research, technological development and demonstration. The SUREBridge project is co-funded by Funding Partners of the ERA-NET Plus Infravation programme.

References

[1] Bakis CE, Bank LC, Brown VL, Cosenza E, Davalos JF, Lesko JJ, et al. Fiber-reinforced polymer composites for construction—state-of-the-art review. J Compos Constr 2002;6:73–87. https://doi.org/10.1061/(ASCE)1090-0268(2002)6:2(73).
[2] Naser MZ, Hawileh RA, Abdalla JA. Fiber-reinforced polymer composites in strengthening reinforced concrete structures: A critical review. Eng Struct 2019; 198:109542. https://doi.org/10.1016/j.engstruct.2019.109542.
[3] Kotynia R, Walendziak R, Stoecklin I, Meier U. RC slabs strengthened with prestressed and gradually anchored CFRP strips under monotonic and cyclic loading. J Compos Constr 2010;15:168–80. https://doi.org/10.1061/(ASCE)CC.1943-5614.0000081.
[4] Hawileh RA, Rasheed HA, Abdalla JA, Al-Tamimi AK. Behavior of reinforced concrete beams strengthened with externally bonded hybrid fiber reinforced polymer systems. Mater Des 2014;53:972–82. https://doi.org/10.1016/j.matdes.2013.07.087.
[5] Linghoff D, Haghani R, Al-Emrani M. Carbon-fibre composites for strengthening steel structures. Thin-Walled Struct 2009;47(10):1048–58.
[6] Colombi P, Poggi C. An experimental, analytical and numerical study of the static behavior of steel beams reinforced by pultruded CFRP strips. Compos B Eng 2006; 37:64–73. https://doi.org/10.1016/j.compositesb.2005.03.002.
[7] Haghani R, Al-Emrani M, Kliger R. Interfacial stress analysis of geometrically modified adhesive joints in steel beams strengthened with FRP laminates. Constr Build Mater 2009;23:1413–22. https://doi.org/10.1016/j.conbuildmat.2008.07.013.
[8] Ghafoori E, Schumacher A, Motavalli M. Fatigue behavior of notched steel beams reinforced with bonded CFRP plates: Determination of prestressing level for crack arrest. Eng Struct 2012;45:270–83. https://doi.org/10.1016/j.engstruct.2012.06.047.
[9] Kliger R, Haghani R, Brunner M, Harte AM, Schober K-U. Wood-based beams strengthened with FRP laminates: improved performance with pre-stressed systems. Eur J Wood Prod 2016;74:319–30. https://doi.org/10.1007/s00107-015-0970-5.
[10] Haghani R, Al-Emrani M, Kliger R. Control of interfacial stresses in beams strengthened with prestressed CFRP laminates. In: Proceedings of the 1st Asia-Pacific Conference on FRP in Structures, APFIS 2007, vol. 2. p. 1053–60.
[11] Motavalli M, Czaderski C, Pfyl-Lang K. Prestressed CFRP for strengthening of reinforced concrete structures: Recent developments at Empa, Switzerland. J Compos Constr 2011;15:194–205. https://doi.org/10.1061/(ASCE)CC.1943-5614.0000125.
[12] Triantafillou T, Deskovic N. Innovative prestressing with FRP sheets: Mechanics of short-term behavior. J Eng Mech 1991;117:1652–72. https://doi.org/10.1061/(ASCE)0733-9399(1991)117:7(1652).
[13] Triantafillou T, Deskovic N, Deuring M. Strengthening of concrete structures with prestressed fiber reinforced plastic sheets. ACI Struct J 1992;89:235–44.
[14] Aslam M, Shafigh P, Jumaat MZ, Shah SNR. Strengthening of RC beams using prestressed fiber reinforced polymers – A review. Constr Build Mater 2015;82: 235–56. https://doi.org/10.1016/j.conbuildmat.2015.02.051.
[15] El-Hacha R, Wight R, Green M. Prestressed fibre-reinforced polymer laminates for strengthening structures. Prog Struct Engng Mater 2001;3:111–21. https://doi.org/10.1002/pse.76.
[16] Yang J, Haghani R, Al-Emrani M. Innovative prestressing method for externally bonded CFRP laminates without mechanical anchorage. Eng Struct 2019;197: 109416. https://doi.org/10.1016/j.engstruct.2019.109416.
[17] Spadea G, Bencardino F, Swamy RN. Structural behavior of composite RC beams with externally bonded CFRP. J Compos Constr 1998;2:132–7. https://doi.org/10.1061/(ASCE)1090-0268(1998)2:3(132).
[18] Garden HN, Hollaway LC. An experimental study of the failure modes of reinforced concrete beams strengthened with prestressed carbon composite plates. Compos B Eng 1998;29:411–24. https://doi.org/10.1016/S1359-8368(97)00043-7.
[19] Karam EC, Hawileh RA, El Maaddawy T, Abdalla JA. Experimental investigations of repair of pre-damaged steel-concrete composite beams using CFRP laminates and mechanical anchors. Thin-Walled Struct 2017;112:107–17. https://doi.org/10.1016/j.tws.2016.12.024.
[20] Smith ST, Teng JG. Shear-bending interaction in debonding failures of FRP-plated RC beams. Adv Struct Eng 2003;6:183–99. https://doi.org/10.1260/136943303322419214.
[21] Al-Amery R, Al-Mahaidi R. Coupled flexural–shear retrofitting of RC beams using CFRP straps. Compos Struct 2006;75:457–64. https://doi.org/10.1016/j.compstruct.2006.04.037.
[22] Kim YJ, Wight RG, Green MF. Flexural strengthening of RC beams with prestressed CFRP sheets: Using nonmetallic anchor systems. J Compos Constr 2008;12:44–52. https://doi.org/10.1061/(ASCE)1090-0268(2008)12:1(44).
[23] Lam L, Teng JG. Strength of RC cantilever slabs bonded with GFRP strips. J Compos Constr 2001;5:221–7. https://doi.org/10.1061/(ASCE)1090-0268(2001)5:4(221).
[24] Eshwar N, Ibell TJ, Nanni A. Effectiveness of CFRP strengthening on curved soffit RC beams. Adv Struct Eng 2005;8:55–68. https://doi.org/10.1260/1369433053749607.
[25] Zhang HW, Smith ST, Kim SJ. Optimisation of carbon and glass FRP anchor design. Constr Build Mater 2012;32:1–12. https://doi.org/10.1016/j.conbuildmat.2010.11.100.
[26] Ali A, Abdalla J, Hawileh R, Galal K. CFRP mechanical anchorage for externally strengthened RC beams under flexure. Phys. Procedia 2014;55:10–6. https://doi.org/10.1016/j.phpro.2014.07.002.
[27] Kalfat R, Al-Mahaidi R, Smith ST. Anchorage devices used to improve the performance of reinforced concrete beams retrofitted with FRP composites: State-of-the-art review. J Compos Constr 2013;17:14–33. https://doi.org/10.1061/(ASCE)CC.1943-5614.0000276.
[28] Grelle SV, Sneed LH. Review of anchorage systems for externally bonded FRP laminates. Int J Concr Struct Mater 2013;7:17–33. https://doi.org/10.1007/s40069-013-0029-0.
[29] Stöcklin I, Meier U. Strengthening of concrete structures with prestressed and gradually anchored CFRP strips. FRPRCS-5: Fibre-reinforced plastics for reinforced concrete structures Volume 1. Thomas Telford Publishing; 2001. p. 291–6. 10.1680/frprcsv1.30299.0030.
[30] Czaderski C, Martinelli E, Michels J, Motavalli M. Effect of curing conditions on strength development in an epoxy resin for structural strengthening. Compos B Eng 2012;43:398–410. https://doi.org/10.1016/j.compositesb.2011.07.006.
[31] Kotynia R, Staskiewicz M, Michels J, Czaderski C, Motavalli M. Pioneering strengthening of bridge girders with pretensioned CFRP laminates in Poland. In: Proceedings of SMAR 2015 the 3rd conference on smart monitoring, assessment and rehabilitation of civil structures; 2015. 8 pp.
[32] Haghani R, Al-Emrani M, Kliger R. A new method for strengthening concrete structures using prestressed FRP laminates. In: Proceeding of the 8th international structural engineering and construction conference; 2015. p. 1153–8.
[33] Haghani R, Al-Emrani M. A new method for application of pre-stressed FRP laminates for strengthening of concrete structures. In: Proceeding of the 19th IABSE Congress, Stockholm; 2016. p. 1556–63.
[34] Naser MZ, Hawileh RA, Abdalla J. Modeling strategies of finite element simulation of reinforced concrete beams strengthened with FRP: A review. J Compos Sci 2021; 5:19. https://doi.org/10.3390/jcs5010019.
[35] Simulia. ABAQUS 6.14: User's Manual. Providence, RI: Dassault Systems; 2014.
[36] CEN. EN 1992-1-1 Eurocode 2: Design of concrete structures - Part 1-1: General ruels and rules for buildings. Brussels: CEN; 2005.
[37] fib. fib Model Code for Concrete Structures 2010. John Wiley & Sons; 2013.
[38] ASTM International. A615/A615M-20 Standard Specification for Deformed and Plain Carbon-Steel Bars for Concrete Reinforcement. West Conshohocken, PA: ASTM International; 2020.
[39] ASTM International. ASTM D3039 / D3039M-17 Standard Test Method for Tensile Properties of Polymer Matrix Composite Materials. West Conshohocken, PA: ASTM International; 2017. 10.1520/D3039_D3039M-17.
[40] Heshmati M, Haghani R, Al-Emrani M. Durability of bonded FRP-to-steel jointsEffects of moisture, de-icing salt solution, temperature and FRP type. Compos B Eng 2017;119:153–67. https://doi.org/10.1016/j.compositesb.2017.03.049.
[41] Mathern A, Yang J. A practical finite element modeling strategy to capture cracking and crushing behavior of reinforced concrete structures. Materials 2021; 14:506. https://doi.org/10.3390/ma14030506.
[42] Bažant ZP, Oh BH. Crack band theory for fracture of concrete. Mat Constr 1983;16: 155–77. https://doi.org/10.1007/BF02486267.
[43] Jirásek M, Bažant ZP. Inelastic analysis of structures. John Wiley & Sons; 2002.
[44] fib. CEB-FIP Model Code 1990: Design Code. fib Fédération internationale du béton; 1993.
[45] Lu XZ, Teng JG, Ye LP, Jiang JJ. Bond-slip models for FRP sheets/plates bonded to concrete. Eng Struct 2005;27:920–37. https://doi.org/10.1016/j.engstruct.2005.01.014.